JOURNAL OF MATERIALS SCIENCE 32 (1997) 5113–5122

Hydrated $K_2SO_4 \cdot 2MgSO_4$ structure revealed by TGA/DTA and magic-angle spinning ^{1}H-NMR spectroscopy

J. ZHANG*, P. A. SMITH, G. R. GOLCAR, L.-Q. WANG AND J. G. DARAB
Chemical Separations and Slurry Processing Group, Pacific Northwest National Laboratory, Richland, WA 99352, USA

The hydration of $K_2SO_4 \cdot 2MgSO_4$ as a function of water addition was examined by pore-size distribution, thermo-gravimetric analysis/differential thermal analysis and nuclear magnetic resonance (NMR) spectroscopy. Thermal studies indicated that the dehydration reactions occur within three distinct temperature regimes which correspond to different degree of hydrogen bonded water or water in different pore-size environments. Solid NMR studies resolved three different proton peaks at each water loading, that represent different chemical environments around water, and also the different range of hydrogen bonding strengths. Therefore, the different chemical environments associated with pore size around water are key factors influencing the NMR spectra. Both thermal and NMR studies suggested that pore size affects the molecular interactions between water and water, and water and the substrate. Also X-ray diffraction studies identified the presence of three phases existing in the hydrated products after the hydration reaction.

1. Introduction

Langbeinite, a naturally occurring mineral, has the formula $K_2SO_4 \cdot 2MgSO_4$. Owing to its environmental benignity, it has been extensively used in waste simulant development at the Hanford site, in southeastern Washington [1]. Specifically, langbeinite has been used as a saltcake simulant and a target material to be retrieved via waterjet cutting [2]. The success of langbeinite as a saltcake simulant material is two-fold: (1) a range of porosities similar to actual waste is possible, (2) the strength of the actual saltcake and langbeinite is derived from hydrogen bonding. Thus, an understanding of the material structure, reactivity, stability, as well as its physical properties, is of importance.

$K_2SO_4 \cdot 2MgSO_4$ reacts with water, and under certain circumstances, forms different types of mineral products. Unlike most other porous materials, such as zeolite, the formation of a cement-like porous material using $K_2SO_4 \cdot 2MgSO_4$ is not through cross-linking nor chemical bonding reactions; instead, water-induced hydration is responsible for the solid growth process. As a result, controlling the process chemistry has a significant impact on the material structure and properties.

Previous studies [3] showed that $K_2SO_4 \cdot 2MgSO_4$ can react with water and form the two minerals, schoenite ($K_2SO_4 \cdot MgSO_4 \cdot 6H_2O$) and epsomite ($MgSO_4 \cdot 7H_2O$). That is

$$K_2SO_4 \cdot 2MgSO_4 + 13H_2O = K_2SO_4 \cdot MgSO_4 \cdot 6H_2O + MgSO_4 \cdot 7H_2O \quad (1)$$

Because many hydrated products (e.g. $K_2SO_4 \cdot MgSO_4 \cdot mH_2O$, $m = 4$ or 6, and $MgSO_4 \cdot nH_2O$, $n = 0, 1, 2, 4, 5, 6, 7$) can be formed, the critical questions are: how are the reaction products controlled, and what are the favourable reaction products under specific conditions?

Studies on various minerals using X-ray diffraction, thermal analysis, and spectroscopies have been reported [3–8]. X-ray diffraction offers information on phase composition and structure. Thermal analysis can provide additional information on material structure, composition, and thermal stability. Spectroscopy, however, gives more insight into molecular level information about molecule–molecule interactions. Combining all the information obtained from these techniques can explicitly elucidate the material physical properties and molecular structure.

The water structure in pure compounds, such as $MgSO_4 \cdot 7H_2O$ and $K_2SO_4 \cdot MgSO_4 \cdot 6H_2O$, was studied extensively by other researchers using different techniques [9, 10]. Sekar *et al.* [9] studied $K_2SO_4 \cdot MgSO_4 \cdot 6H_2O$ compound using infrared and polarized Raman spectroscopy and resolved three different water molecules with different strengths of bonding with Mg^{2+}. Ferraris *et al.* [10] investigated $MgSO_4 \cdot 7H_2O$ using neutron diffraction. In epsomite, SO_4^{2-} tetrahedra and $Mg(H_2O)_6^{2+}$ octahedra are linked by hydrogen bonds which also involve the seventh water molecule, which is not coordinated to Mg^{2+}. As a result, the dehydration of $MgSO_4 \cdot 7H_2O$

*Author to whom all correspondence should be addressed.

0022–2461

can give rise to a series of natural mineral products depending on the strength of the hydrogen bonding. The differences in molecular bonding may or may not be detected by the thermal analysis method depending on whether the operation conditions (temperature and pressure) favour a specific bond-dissociation energy.

We primarily investigated $K_2SO_4 \cdot 2MgSO_4$ hydrated compounds using X-ray diffraction, porosimetry, simultaneous thermogravimetric analysis–differential thermal analysis–mass spectrometry (TGA–DTA–MS), and nuclear magnetic resonance (NMR) techniques. In this paper, we address (1) water molecule incorporation into the porous monolith; (2) the degree of hydration of $K_2SO_4 \cdot 2MgSO_4$ as a function of added water content, and (3) the temperature effect on the degree of hydration and phase compositions.

2. Experimental procedure

Potassium magnesium sulphate (langbeinite, $K_2SO_4 \cdot 2MgSO_4$, 97.3%, Pitman-Moore Company) was used as-received. Samples were prepared with added water (varied from 10–30 wt%), and then cured at room temperature at 100% relative humidity over 3 weeks. The added amount of water at higher percentages was not completely reacted with langbeinite; the water remaining in the samples after the 3 week curing was discarded, and samples were then kept at 100% relative humidity for another week. For the sample prepared at a higher temperature (100 °C), 66.7 wt % water was added, and then the sample was heated to 100 °C for 5 min. Under these conditions, a saturated dissolution of the solid was achieved. The sample was cooled and cured at room temperature with 100% relative humidity over 3 weeks. Extra water in the sample container was discarded afterwards. In this paper, all water weight percentages mentioned are the added water weight per cents instead of the consumed water weight per cents.

The cured samples were used for all X-ray diffraction, pore-size distribution, thermal analysis, and NMR experiments. For X-ray diffraction (XRD) measurements, samples were ground to a size of about 75 microns. The powder samples were analysed with a Philips X-ray diffractometer (Mahwah, NJ PN 3550100 × wide-range goniometer and model XRG 3100 X-ray generator) using CuK_α (40 kV/45 mA) radiation.

Mercury porosimetry measurements (Pore Sizer 9305, Micromeritics, Norcross, GA) were performed on the previously described samples. The pore radius, R, is related to the intruding mercury pressure, P_i, by the Washburn equation [11]

$$P_i = -2\gamma \cos\theta / R \quad (2)$$

where g and q are the surface tension and contact angle of the mercury, respectively. The reported pore-size distributions were obtained during mercury intrusion. The pore volume fraction was obtained by measuring the maximum volume of mercury intruded. The average pore radii reported were obtained from the peak maxima on the differential pore volume curves.

Simultaneous TGA–DTA–MS (SDT 2960, TA Instrument) was used to measure the weight loss from a sample and the temperature change due to the reaction while heating over a given temperature interval. All samples were ground into very fine powder prior to thermal experiments. The experimental conditions, such as heating rate (10 °C min^{-1}), particle size, sample holders and sample size (ranged from 14–18 mg), and furnace pressure, were kept consistent in all measurements to obtain systematic results.

NMR experiments were carried out on the Chemagnetics solid-state NMR spectrometer (300 MHz–89 mm wide-bore Oxford Magnet) using a double resonance probe. Samples were loaded into a 5 mm Zirconia Pencil™ rotor spun at 10–12 kHz. Spectra were collected by using a single-pulse block-decay method with a 4.5 ms (90°)^{1}H pulse, and a 5 s repetition delay. For all experiments, a 40 ms acquisition time and a 50 kHz spectral window were employed. The number of transients ranged from 50–100. Line broadening of 24 Hz was used for all spectra. The chemical shift of each spectrum was referenced to tetramethylsilane (TMS).

3. Results and discussion

3.1. Structure and phase composition revealed by X-ray diffraction

X-ray diffraction is a very useful technique in quantitative determination of structure and phases because the intensities of the diffraction peaks of a given compound in a mixture are related to the fraction of the material in the mixture. However, direct comparison of the intensity of a diffraction peak in the pattern obtained from a mixture is fraught with difficulties. Here, we applied an X-ray diffraction method to gain qualitative information on the composition of phases. A series of X-ray diffraction patterns were obtained for samples with different amounts of added water ranging from 10–30 wt %. From water content-dependent studies, the effect of added water quantity on the extent of the hydration reaction was determined.

X-ray diffraction studies suggest that the hydration of potassium magnesium sulphate follows a reaction

$$K_2SO_4 \cdot 2MgSO_4 + 10H_2O = K_2SO_4 \cdot 2MgSO_4 \cdot 4H_2O + MgSO_4 \cdot 6H_2O \quad (3)$$

Over the range of water contents added to the samples, three major phases, $K_2SO_4 \cdot 2MgSO_4$ (starting phase), $K_2SO_4 \cdot MgSO_4 \cdot 4H_2O$ and $MgSO_4 \cdot 6H_2O$, were identified without exception. However, the insignificant amount of additional trace phase ($MgSO_4 \cdot 4H_2O$) in some samples can probably be attributed to (1) the sensitivity of the measurement method; and (2) a small variation from the samples. The presence of this phase ($MgSO_4 \cdot 4H_2O$) was neglected here because of its small contribution (1%–2%) and the absence of this phase in most samples.

X-ray diffraction studies qualitatively show that the amount of added water (10–30 wt %) does not change the composition of the reaction products. To reveal

the temperature effect on this reaction, a sample prepared at higher temperature (100 °C) and water loading (66.7 wt %) was also examined. At higher water loading and temperature, langbeinite has a higher solubility. Under these experimental conditions, the precursor contains two phases: undissolved solid phase and supersaturated salt solution. The final cured sample has two different (visually) apparent phases, the major solid phase (about 98 wt %) from the undissolved sample through the hydration reaction and a small amount of crystal phase (2 wt %) recrystallized from the supersaturated solution. X-ray analysis of these two phases gave very different diffraction patterns. Surprisingly, the bulk solid phase also contains the same three phases as samples prepared at room temperature. However, the crystal phase from the supersaturation is completely due to formation of a new phase, $K_2SO_4 \cdot MgSO_4 \cdot 6H_2O$.

If the solid growth proceeds by a dissolution/precipitation mechanism, the degree of the hydration reaction is not very dependent on water loading and temperature because X-ray diffraction studies showed the same phase compositions and structure in all samples. However, the hydrated compound can be different if the reaction mechanism is through crystallization, because crystal growth from supersaturated ionic solution occurs by a series of consecutive steps: bulk diffusion, surface adsorption, surface diffusion, surface reaction, and integration of ions or molecules into the crystal lattice, leading to the formation of a different solid phase.

3.2. Pore-size measurements

Through the hydration mechanism, porous materials of potassium magnesium sulphate are generated. Before determining how the addition of water affects the interactions between water–water, and water–substrate, and affects the local water environment, pore-size measurements were conducted. We expected to link these results with thermally induced dehydration reactions and the degree of hydrogen bonding present in the hydrated materials.

The same set of samples (10–30 wt % water) were used for pore-size measurements. Fig. 1 shows the different pore-size distributions obtained from our measurement for 18 wt % added water. Two main size distributions were observed continuously through the entire range of water loadings. The large pore size has a predominant contribution to the average pore size in these porous materials. The average pore size derived from these pore-size distributions versus water content is then given in Fig. 2. The average pore size varies with the addition of water in such a way that at lower water loading (12 wt %), large pore-size distribution dominates the average pore size. As more water is incorporated into the sample, the pore-size distribution shifts towards smaller sizes, leading to a decrease in the average pore size. The average pore diameter does not change when the water loading is greater than 14 wt %. The variation in pore size with the addition of water is attributed to the increased dissolution of solid with increasing water content

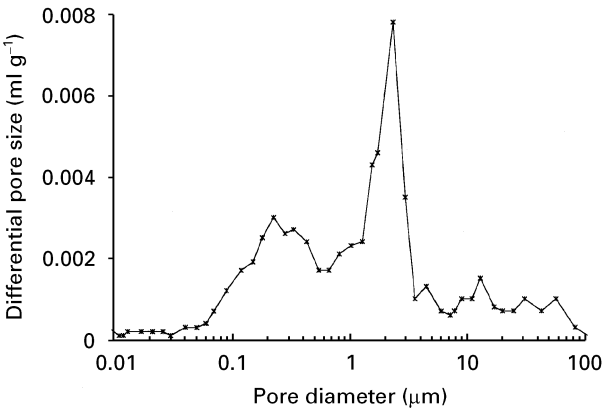

Figure 1 Pore-size distribution from porosimetry measurement for 18 wt % water loading.

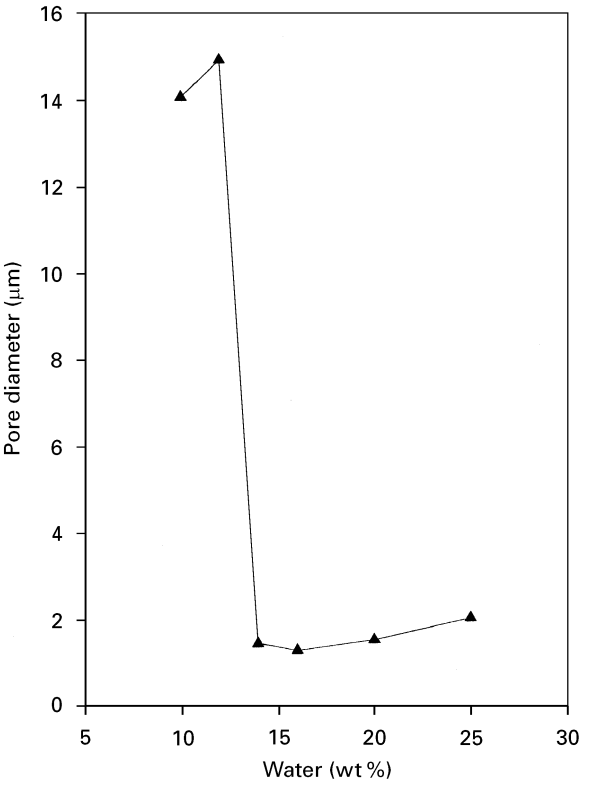

Figure 2 Average pore size versus addition of water (ranging from 10–30 wt %).

which significantly changes the particle size and its shape, leading to a more effective particle contact and a smaller pore size. Above 14 wt % water loading, dissolution of the solid in water produces very uniform size of particles, and further increasing the water loading only diminishes the number of these uniform particle sizes, therefore, particle size is no longer controlling the particle packing, as well as the pore size.

3.3. Thermal treatment and analysis

3.3.1. Effect of water on the degree of hydration at room temperature

Qualitative analysis from XRD indicates the number of phases that result from the hydration reaction. However, knowledge is still lacking on how the water

molecules bond to the substrate and how strong these bonding interactions are. Preliminary thermal analysis tests showed that our experiments were characteristic of dehydration reactions because off-gas analysis using a mass spectrometer demonstrated that water vapour was the only gas evolved. Generally, endothermic reactions include phase transitions, dehydration, reduction, and some decomposition reactions. Similarly, we observed endothermic reactions in all cases for these dehydration reactions. Fig. 3 shows a typical example of DTA for 10 wt % water loading.

Fig. 4 shows TGA plots of the thermally induced weight loss (wt %) as a function of water content up to 30 wt %. Very interestingly, there are three water desorption reactions over the temperature range 80–200 °C in all samples with 10–30 wt % water loadings. The three peaks were attributed to three different types of water, bonding differently to the substrate molecules. The difference in the dehydration temperature could be due to either the difference in the water environment, such as different rigidity caused by different pore sizes, or the different bonding interactions between water molecules and the substrate (e.g. different degree of hydrogen bonding). There are also some changes in the peak position and magnitude of the weight loss of these three peaks as a function of water content.

From TGA at multiple water loadings, the total weight loss (Fig. 5a) and the fractional contribution of each weight loss to the total (Fig. 5b) as a function of water content, were summarized. These were in a good agreement with Fig. 2, that a complete hydration reaction is achieved around a water loading of

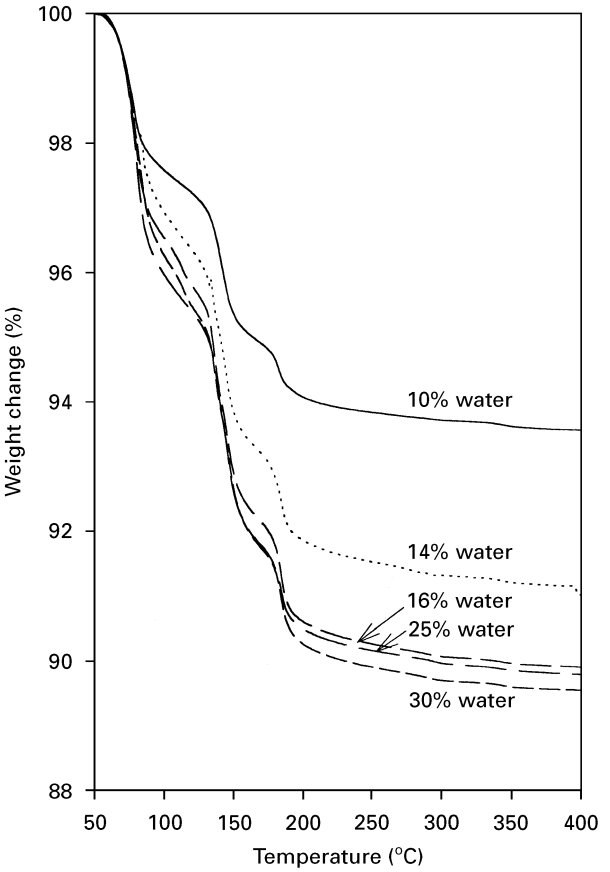

Figure 4 Thermogravimetric analysis of hydrated samples (10–30 wt % water).

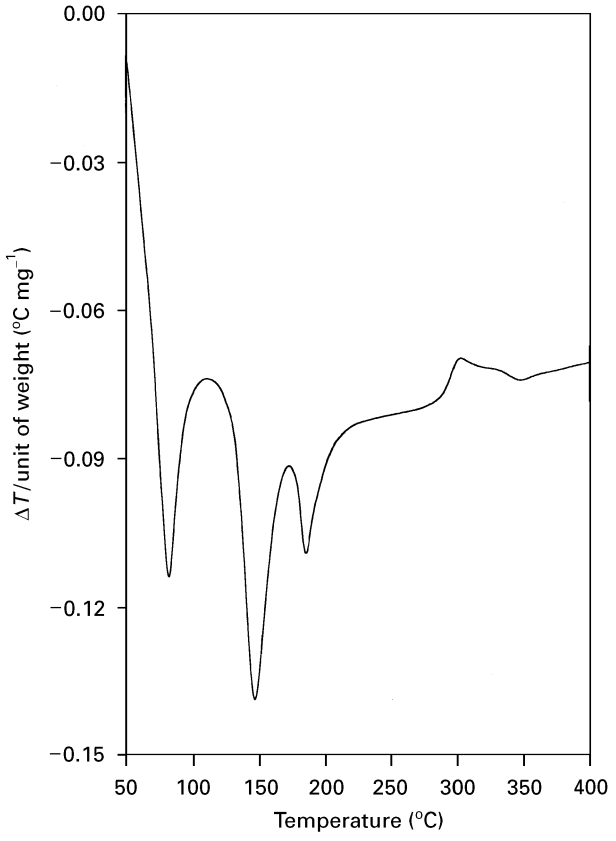

Figure 3 Differential thermal analysis of 10 wt % water loading as a function of furnace temperature.

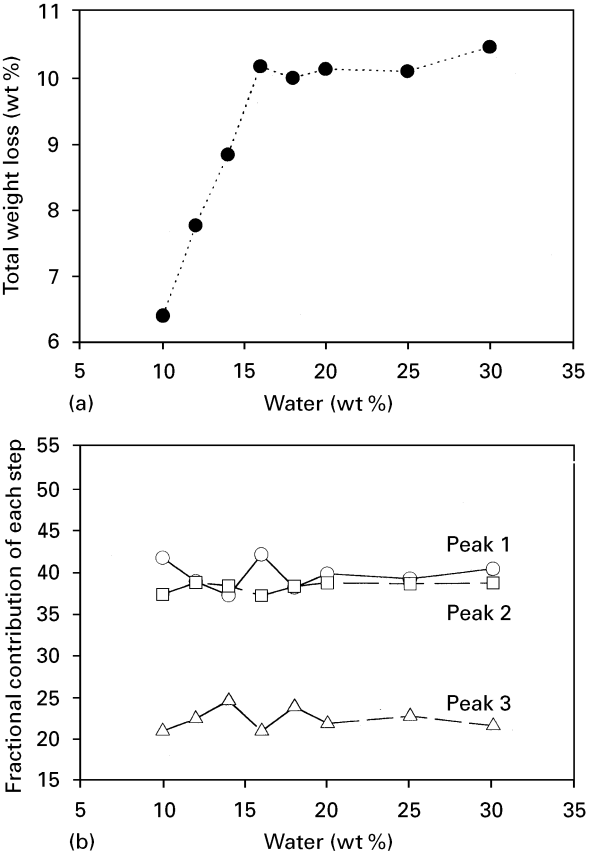

Figure 5 (a) Total weight loss percentage and (b) each peak fractional contribution, as a function of added water.

16 wt %, and no further water is incorporated into the sample, but that dissolution occurs with the addition of water to 30 wt %, leading to the unchanged total weight loss when the water loading is >16 wt %. Fig. 5b also shows that the predominant contribution to the total dehydration process is from the first and second peaks. The fractional contribution of each peak is invariant with addition of water over the entire range of water loadings (10–30 wt %), indicating that the partitioning of water into each domain does not happen.

The ratio of peaks 1, 2, and 3 in Fig. 5b is 2:2:1, and does not change with water content up to the water loading of 30 wt %. The question is: are these three peaks from different chemical bonds within a molecule, or from different pore-size environments? If the thermally induced dehydration reaction is due to the difference in intramolecular hydrogen bonding in a hydrated compound, it is reasonable to assume that the first peak (80–90 °C) is the liberation of four molecules of water from $K_2SO_4 \cdot MgSO_4 \cdot 4H_2O$, the second is another four molecules of water from $MgSO_4 \cdot 6H_2O$, and the third is last two molecules of water from $MgSO_4 \cdot 6H_2O$. To test our hypothesis, thermally treated samples with 20 and 30 wt % water loadings at 130 and 170 °C, respectively, were subjected to X-ray diffraction analysis. X-ray diffraction analyses from these thermally treated samples show that the phase compositions ($K_2SO_4 \cdot 2MgSO_4$, $K_2SO_4 \cdot 2MgSO_4 \cdot 4H_2O$, $MgSO_4 \cdot 6H_2O$) at both water contents and temperatures remain the same as those samples without thermal treatments. Thus, XRD results from the two thermally treated samples demonstrate that the thermally induced liberation of water is not attributable to the differential intramolecular hydrogen bonding, but instead to the second possibility, where different intermolecular hydrogen bonding or interactions due to the different environments around the water, may play a key role in determination of the thermally dependent dehydration reactions.

Fig. 6 shows the endothermic peak shift of samples as a function of water content. All three peaks shift towards higher temperature with increasing water content. The largest shift was observed for the first peak (80–88 °C) which is about 10% of the total increment. The second peak (145–150 °C) has a relatively smaller shift (about 4%); the peak positioned in the highest temperature region (184–188 °C) has the smallest shift (only about 2%). From our thermal analyses, we anticipate that water content-dependent pore-size change is responsible for the thermally induced dehydration reactions. The rigidity of the water environment is controlled by the pore size. The shift of the peak towards higher temperatures was attributed to decreased pore size. The initial dissolution and subsequent re-precipitation results in a smaller particle size and ultimately, a smaller pore size in the sample. As a result, a more rigid water environment with increasing water content will be expected, leading to a small shift in the thermal peak positions. However, we did not observe a significant change in the peak temperature around 14 wt % water even through a large change in average pore diameter at 14 wt % water was observed (Fig. 2).

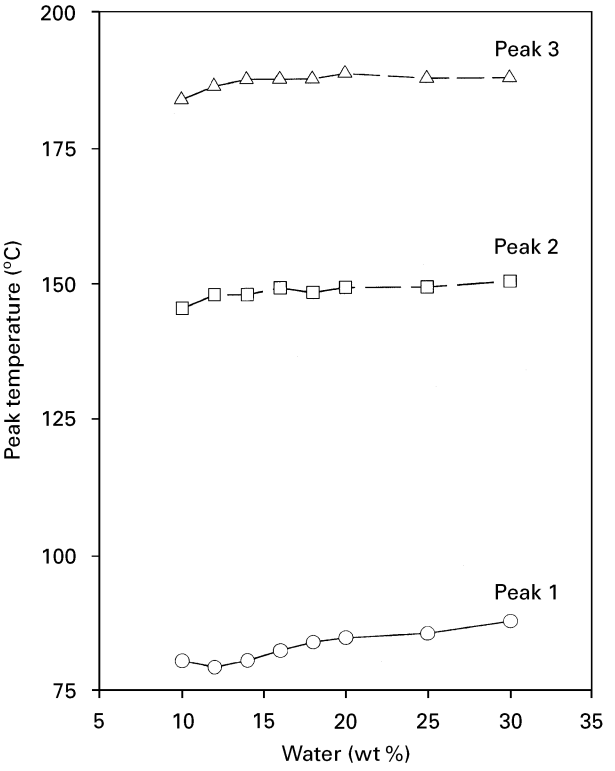

Figure 6 Peak temperature for three endothermic peaks as a function of added water.

3.3.2. Effect of temperature on the degree of hydration

Temperature is a very important factor in controlling physical and chemical reactions. From the kinetics standpoint, increasing temperature increases the reaction rate (dynamic effect) significantly. Thus, the reacting species can contact each other more completely and effectively. Another concern in our temperature studies was to change the solubility of the samples [12] so that the degree of hydration, particle size and packing density could be manipulated.

Temperature and concentration gradients are both very important in the determination of crystal phase and structure. We prepared a $K_2SO_4 \cdot 2MgSO_4$ sample with a higher water loading (66.7 wt %) and at 100 °C. At this temperature, more solid dissolves in the aqueous phase and supersaturation is achieved as the temperature is brought to room temperature. The sample cured at room temperature over 3 weeks was then used for thermal analysis.

Two different solid phases were observed visually: a transparent phase on the surface and a light pink phase in the bulk. DTA/TGA experiments of both phases were conducted. The difference in thermal reactions is very significant (Fig. 7a and b). In Fig. 7a, a single-step reaction from the transparent surface phase was observed, whilst multiple-step reactions for the bulk light-pink phase were resolved, which are very similar to those samples prepared at room temperature. As we discussed earlier, X-ray diffraction analysis suggests that the single-crystal phase from the transparent surface layer was $K_2SO_4 \cdot MgSO_4 \cdot 6H_2O$. Quantitative thermal analysis agrees well with the presence of a single-phase compound, $K_2SO_4 \cdot MgSO_4 \cdot 6H_2O$,

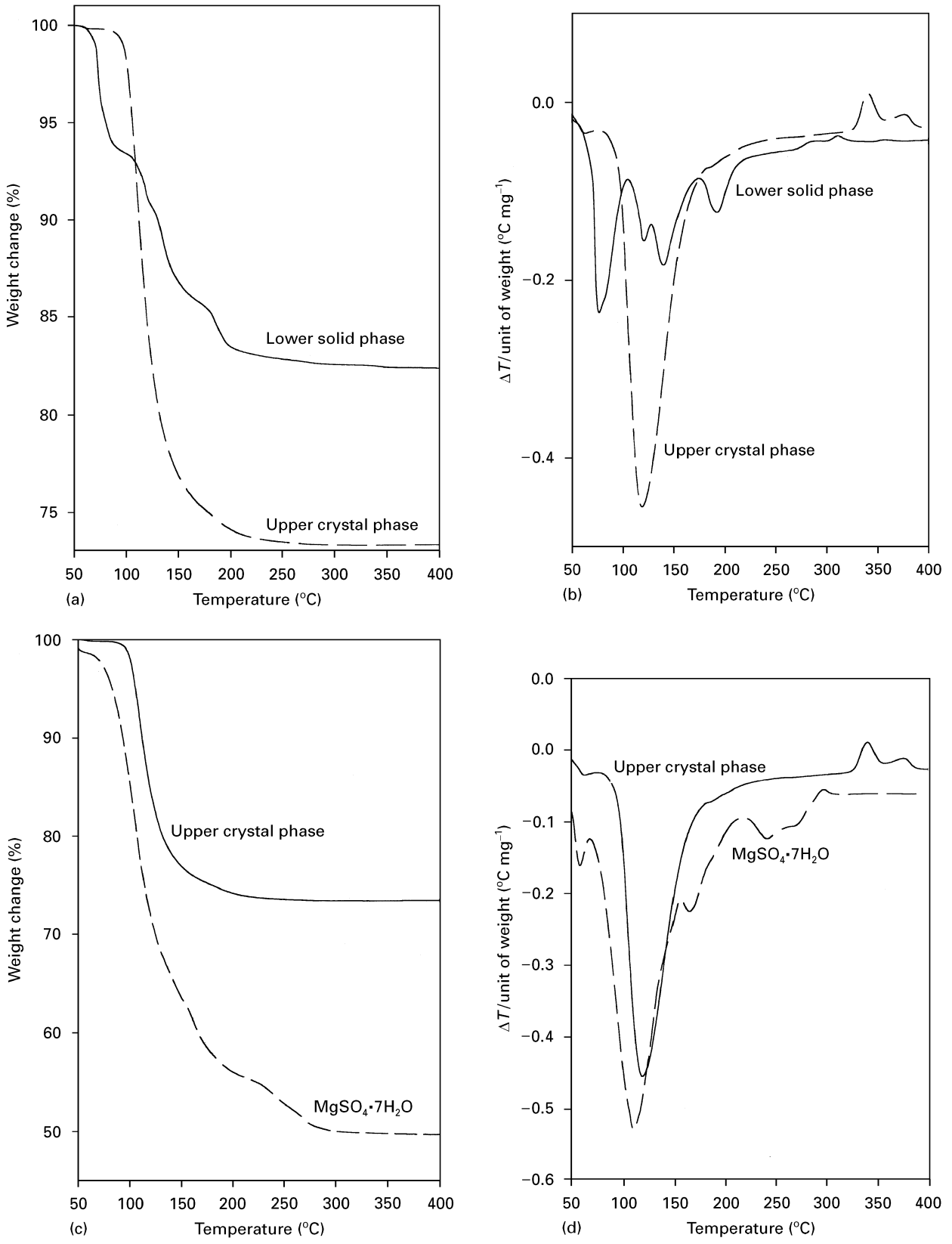

Figure 7 (a) TGA of lower and upper phases from the sample with the addition of 66.7 wt % water, heated at 100 °C and cured at room temperature. (b) DTA of the same sample as (a). (c) Comparison of the TGA spectra of the obtained crystal phase, $K_2SO_4 \cdot MgSO_4 \cdot 6H_2O$, with the commercially purchased $MgSO_4 \cdot 7H_2O$. (d) Comparison of DTA plots of the obtained crystal phase, $K_2SO_4 \cdot MgSO_4 \cdot 6H_2O$, with the commercially purchased $MgSO_4 \cdot 7H_2O$.

because the total weight loss obtained from Fig. 7a is around 27%, which is the same as the calculation of $((6MW_{H_2O}/MW_{K_2SO_4 \cdot MgSO_4 \cdot 6H_2O}) \times 100\% = (108/402.7) \times 100\% =)$ 27% if all six waters dehydrate at once (MW is the molecular weight). The lower bulk solid phase, however, maintains similar features to those prepared at room temperature, although a small peak split takes place in the second peak. Fig. 7b depicts more clearly the differential thermal behaviour of these two samples. (1) The thermal behaviour of the

lower bulk solid phase resembles that of other samples prepared at room temperature, indicating that the phase composition of these samples prepared under different conditions (water percentage and temperature) are similar. (2) Three significant dehydration steps with intensity ratios of 2:2:1 from the lower solid phase are assigned as the loss of 40% of the free water absorbed on the surface or within the large pore in the first temperature region, 40% of the hydrate water with some degree of hydrogen bonding within the large pore in the second temperature region, and the last 20% of the hydrate water within a very rigid environment or small pore in the third temperature region. The second peak was split into two peaks which may indicate the similarity of the water environments. (3) A single-step weight loss for the transparent surface phase obtained from the supersaturated solution reflects not only the homogeneity of the hydrated material but also the degree of hydration in the $K_2SO_4 \cdot MgSO_4 \cdot 6H_2O$ (e.g. six hydrated waters of each molecule). No indication of these six hydrated waters bonding differently with Mg^{2+} ions from the thermal analysis, was observed.

Fig. 7c and d compare TGA/DTA of $K_2SO_4 \cdot MgSO_4 \cdot 6H_2O$ from the transparent surface phase with the commercially purchased $MgSO_4 \cdot 7H_2O$. The latter contains seven hydrated waters which exhibit different thermal behaviour. Over the entire dehydration process, three major reaction regions were observed for $MgSO_4 \cdot 7H_2O$. The predominant reaction occurs at 115 °C where five hydrated waters are lost. The second (160 °C) and third (240 °C) peaks represent one hydrated water each. A small peak around 60 °C in Fig. 7d was attributed to an instrument artefact, because this peak can be observed in all samples. Comparison of the thermal analyses of $K_2SO_4 \cdot MgSO_4 \cdot 6H_2O$ and $MgSO_4 \cdot 7H_2O$ suggests that a different chemical environment for H_2O exists in the $MgSO_4 \cdot 7H_2O$ compound but not in $K_2SO_4 \cdot MgSO_4 \cdot 6H_2O$.

Crystal growth can occur by a variety of mechanisms. For example, crystals can grow by addition of molecules or individual ions that subsequently react and/or become incorporated into the crystal lattice. For ionic solutions, all steps including bulk diffusion, surface adsorption, etc., play important roles in the determination of crystal structure and phases. Thus, the crystal structure and phase obtained from undissolved solid phase and supersaturated solutions are very different in our studies. From the above discussion, it can be concluded that the amount of added water changes the quantity of hydrated products but not the degree of hydration. However, temperature-assisted supersaturation can change the phase composition and solid homogeneity more effectively.

3.4. Water environment revealed by NMR spectroscopy

The addition of water to potassium magnesium sulphate has profound effects on its physical and chemical properties. From the previous discussion of thermal and X-ray diffraction analyses, phase composition and degree of hydration have been explained. However, we still lack an understanding of the difference in molecular interactions between water and water, and water and substrates.

In general, NMR experiments on solid samples are encumbered by the severe line-broadening effects due to strong nuclear–nuclear dipolar interactions [13–19]. If these effects are not too large because of large internuclear distances and/or fast motion averaging, then sharp NMR resonances can often be achieved by the magic-angle spinning (MAS) technique, which can also eliminate the peak broadening caused by chemical shift anisotropy. In this paper, we describe details of our studies using the fast MAS (10–12 kHz) technique on hydrated potassium magnesium sulphate.

NMR experiments were performed on three hydrated samples with 12, 18, and 30 wt % added water. Fig. 8 depicts the NMR spectrum for the 12 wt % water sample. Similar spectral features were also observed for 18 and 30 wt % water samples. In addition, we compared these results with the temperature-assisted supersaturated phase, $K_2SO_4 \cdot MgSO_4 \cdot 6H_2O$, and the commercially purchased compound, $MgSO_4 \cdot 7H_2O$. Fig. 9 shows the NMR spectrum of $K_2SO_4 \cdot MgSO_4 \cdot 6H_2O$.

A number of peaks observed in NMR spectra are attributed to different physical and chemical environments. Three deconvoluted ^1H NMR spectra as shown in Fig. 8 reveal that there are three different types of water in the potassium magnesium sulphate hydrated material. The differences in water behaviour are due to different extents of chemical bonding interactions. Chemical shift, full-width at half-maximum (FWHM), as well as the integrated peak area (%) can thus characterize the hydrated water environments.

Table I summarizes the analysed results from ^1H MAS-NMR experiments for 12, 18 and 30 wt % water. At 12 wt % water, we resolved three peaks at 5.46, 5.55, and 1.44 p.p.m., respectively. When continuously adding more water into the sample (e.g. 18 wt % H_2O), three peaks (5.57, 6.01, and 1.33 p.p.m.) remain. The chemical shift of these three peaks does not change significantly. However, both the integrated peak area (%) and FWHM change as a function of water addition. On increasing the water content to 30 wt %, three peaks (5.46, 6.19 and 1.43 p.p.m.), were still observed, and both integrated peak area (%) and FWHM change correspondingly.

First, these three peaks in NMR spectra represent three different chemical environments around the water. The first sharp peak (5.46–5.57 p.p.m.) at all water loadings was assigned as a highly mobile hydrated water present in the samples. The higher mobility of water can be related to either the weaker interactions between water and water, and between water and the substrate or more flexible water environments (similar to bulk water). The change in the chemical shift of the first peak (5.46–5.57 p.p.m.) as a function of water loading is not significant, indicating only a small effect of added water on the chemical environments of the mobile hydrated water. However, the fraction of this peak with the addition of water

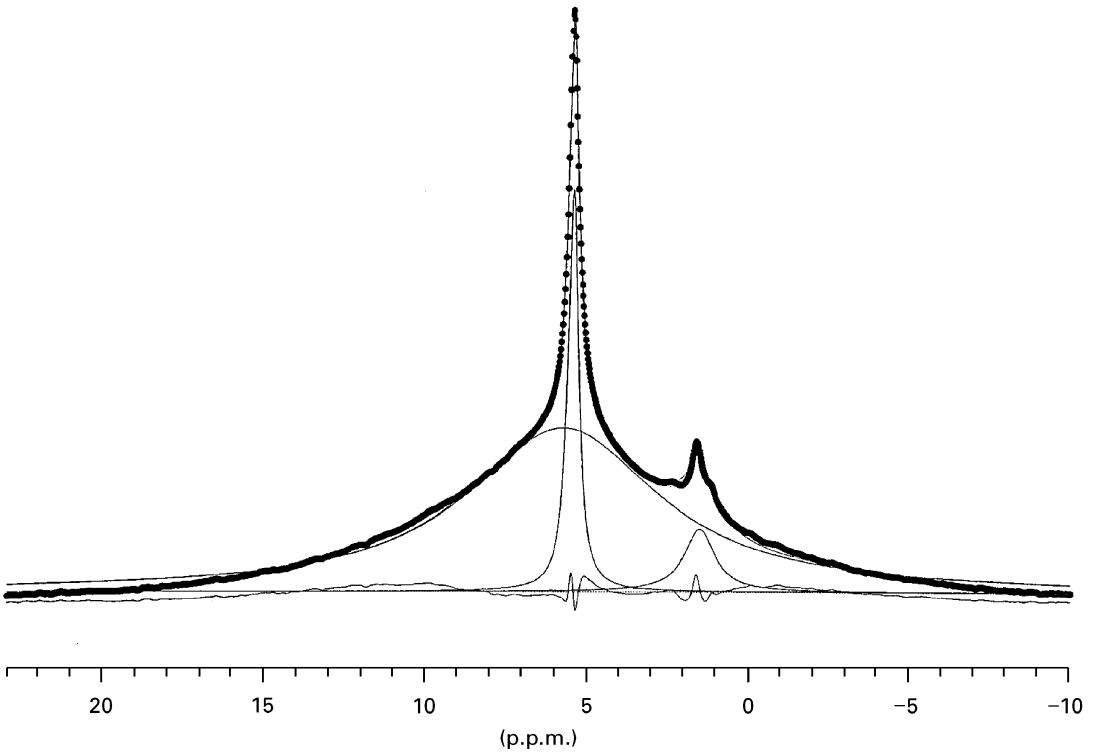

Figure 8 ^{1}H MAS-NMR spectra of langbeinite with 12 wt % water added. (···) Computer synthesized convoluted curve fit to the experimental curve. Three deconvoluted spectra are obtained, as indicated in the figure.

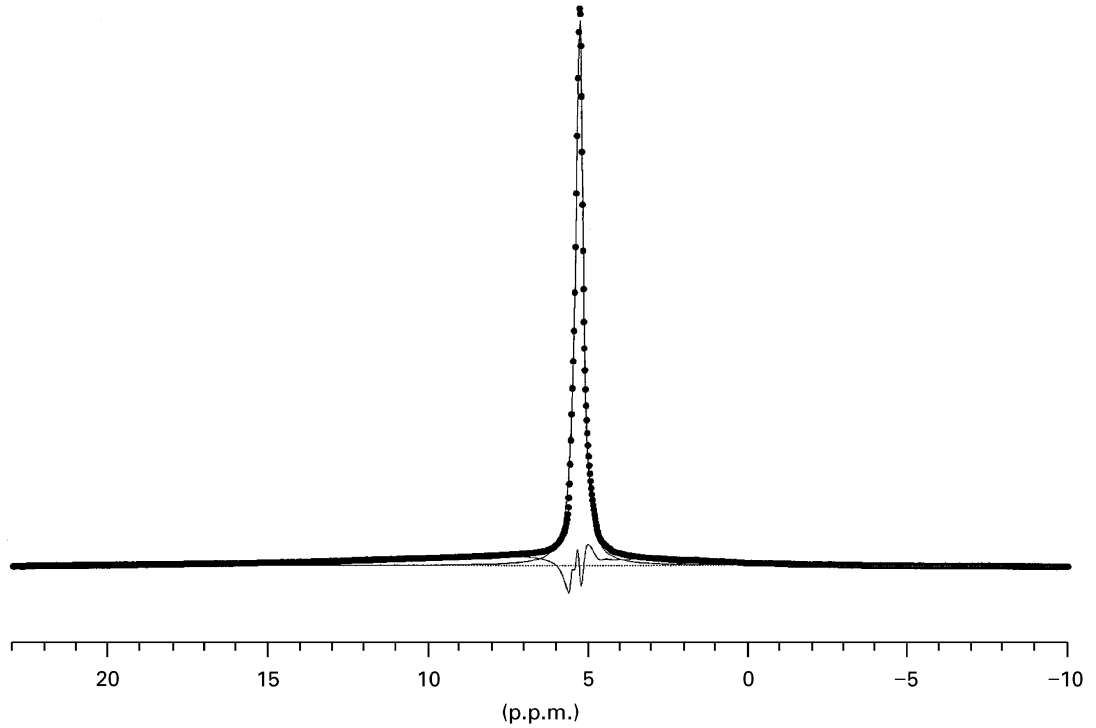

Figure 9 ^{1}H MAS-NMR spectrum of $K_2SO_4 \cdot MgSO_4 \cdot 6H_2O$ obtained from supersaturation of langbeinite (66.7 wt % water at 100 °C). Only a single environment of water was found.

continuously decreases (from 14.3% to 3.3%) with increasing water (from 12 wt % to 30 wt %). This is probably because: (1) pore size decreases with increasing water, resulting in a smaller population of mobile hydrated water, and/or (2) the fraction of hydrogen-bonded hydrated water increases due to the increase in the ratio of H_2O/pore size. The FWHM increases with increasing water addition, suggesting that an

TABLE I Results from ^{1}H MAS-NMR spectroscopy

Peaks	Chemical shift (p.p.m.)			Integrated area (%)			FWHM (Hz)		
	12%	18%	30%	12%	18%	30%	12%	18%	30%
First	5.46	5.57	5.46	14.3	10.7	3.3	121	430	829
Second	5.55	6.01	6.19	81.4	86.2	94.0	2519	2690	1605
Third	1.44	1.33	1.43	4.3	3.1	2.7	269	359	527

increase in environment rigidity, and/or in heterogeneity around mobile hydrated water, leads to a broader chemical shift distribution.

The second peak (5.55–6.19 p.p.m.), however, has a position similar to the first one but a much wider peak width. This peak was probably due to hydrated water with extensive hydrogen-bonding characters in a number of different rigidity environments. The similar positions of the first and second peaks indicate that most of the water represented in the second broad peak is in similar chemical environments to the first one. However, the broad second peak is ascribed to inhomogeneous broadening associated with a wide distribution of chemical shifts that reflect a wide variety of hydrogen-bonding details and strengths. Also, the integrated area of the second peak ($>80\%$) indicated the majority of water is associated with different extents of hydrogen bonding in the samples. It is very important to realize that this broad NMR peak may cover water residing in small and/or large pores, and even on the surface where a wide distribution of hydrogen bonding exists. In addition, the integrated area (%) of this peak increases with increasing water addition, because a decrease in average pore size or an increase in the ratio of H_2O/pore size with increasing water addition enhances the hydrogen bonding strength present in the hydrated water. However, the change in FWHM with water addition is not as we anticipated. This is probably because at a higher water loading (e.g. 30 wt %), higher dissolution and re-precipitation of the chemical produce a more homogeneous material which, in turn, decreases its chemical anisotropic effect.

Finally, the third peak (1.33–1.43 p.p.m.) with $<5\%$ total water, is probably attributed to isolated mobile water. The chemical shift of this peak does not change very much with addition of water, while the fraction of its integrated area slowly decreases with increasing water. The peak FWHM gradually increases with the addition of water, possibly because of increased rigidity around the water environment.

Processing conditions have significant effects on the material microstructure. When potassium magnesium sulphate solid was prepared by adding the solid sample to water (67 wt %) at 100 °C and stirring for about 5 min, supersaturation was achieved, and a transparent crystal phase on the top layer was identified as $K_2SO_4 \cdot MgSO_4 \cdot 6H_2O$ from X-ray diffraction analysis, and clarified by thermal analysis. All six hydrated water molecules were liberated in a single-step dehydration reaction after heating, suggesting the presence of an uniform water environment. Very interestingly, our NMR spectrum (Fig. 9) showed a very narrow and sharp peak at 5.46 p.p.m. which is in a similar position to the first peak (5.46–5.57 p.p.m.) in our samples without temperature treatment (Table I). Again, this supports that all six waters in $K_2SO_4 \cdot MgSO_4 \cdot 6H_2O$ are mobile hydrated water, and have a homogeneous environment.

To illustrate further the effects of chemical environment on ^{1}H NMR spectra, we also collected the ^{1}H NMR spectrum of the commercially available compound, $MgSO_4 \cdot 7H_2O$. Two peaks were observed in this study. The broad peak (at 6.06 p.p.m., FWHM = 1364 Hz) is attributed to hydrogen bonding associated hydrated water, whilst the narrow and sharp one (5.63 p.p.m., FWHM = 79.6 Hz) is ascribed to mobile hydrated water. The broad peak in this sample does not occupy exactly the same position as the first peak given in Table I but is very close to it. The large degree of hydrogen bonding probably changes the peak position as well as the FWHM, resulting in a much wider resonance peak for $MgSO_4 \cdot 7H_2O$.

4. Conclusion

Hydrated compounds formed by langbeinite were characterized using X-ray diffraction, porosimetry, thermal analysis, and NMR techniques. Hydration reactions as a function of added water content and temperature were both studied. Phase composition studies from X-ray diffraction analysis showed that the degree of hydration reactions is not dependent on the water content. However, changing the processing temperature leads to the presence of a new phase which is a more homogeneous hydrated compound, $K_2SO_4 \cdot MgSO_4 \cdot 6H_2O$.

Thermal analysis for these hydrated compounds gives more insight into the temperature-induced dehydration reactions. Three dehydration steps are present in all samples in the temperature range 50–400 °C. The first peak was attributed to free or less-bonded water in each sample, and the other two thermally induced dehydration peaks represented hydrated water in pores of different size and with differing extents of hydrogen bonding. Qualitatively, we found all of the three weight-loss peaks to shift towards higher temperature regions corresponding to the formation of less porous hydrated materials. Also, the unchanged total weight loss due to the liberation of water with the addition of water, for >16 wt % water, may be attributed to either a

completion of the hydration reaction or the existence of structural water which can be released only at a higher temperature.

In contrast, the NMR technique emphasizes both physical (e.g. pore size) and chemical environments (e.g. hydrogen bonding) on the inter- or intramolecular interactions. Our MAS-NMR results support the presence of multiple water environments, and these environments can be attributed to some water in large pores with less or no hydrogen bonding, generally giving rise to a larger mobility, and a sharp NMR peak. In comparison, water in small pores experiences a more rigid environment, a strong hydrogen-bonding interaction, and a slower motion, resulting in a broad resonance peak. The number of NMR peaks indicates how many different types of water are present in the system; the NMR peak width, however, is a distribution of all possible water environments. It is worth mentioning that the peak broadening due to chemical anisotropy can be attributed to either water in different sized pores or water in similar pores with different degrees of hydrogen bonding. As more water is added, the pore size of the hydrated material decreases, and the NMR spectra continuously change (either narrower or wider depending on the peak feature). This observation is in good qualitative agreement with pore-size measurements.

Acknowledgements

This work was supported by the US Department of Energy under contract DE-AC06-76RLO 1830. The authors thank Dr J. Cowin, PNNL, for helpful suggestions in thermodynamic calculations, and Dave McCready for assistance in XRD data acquisition. Pacific Northwest National Laboratory is operated by the Battelle Memorial Institute.

References

1. G. R. GOLCAR, J. R. BONTHA, J. G. DARAB, M. R. POWELL, P. A. SMITH and J. ZHANG, "*Retrieval Process Development and Enhancements Project FY 95 Simulant Development Technology Task progress Report*", PNNL-11103 Pacific Northwest National Laboratory, Richland, Washington, USA (1996).
2. D. A. SUMMERS, *The New York Times Science* January 10 (1995) B5.
3. D. V. GREBENYUK, N. P. OPANASIK, R. P. KOZEL'SKII, N. N. PODOBAILO and V. I. DAVYBIDA, *J. Appl. Chem. USSR* **55** (1982) 1294.
4. D. M. THOMLEY and T. J. PRINIMER, *Clay Mineral.* **30** (1995) 27.
5. M. CALLERI, A. GAVETTI, G. IVALDI and M. RUBBO, *Acta Crystallogr.* **B40** (1984) 218.
6. M. GOTO, B. MOLONY, M. J. RIDGE and G. W. WEST, *Aust. J. Chem.* **19** (1966) 313.
7. M. RUBBO, D. AQUILANO and M. FRANCHINI-ANGELA, *J. Crystal Growth* **71** (1985) 470.
8. J. MAYER, F. GIBLIN, J. HENDERSON and W.-D. EMMERICH, *Ceram. Ind.* **October 143** (1994) 41.
9. G. SEKAR, V. RAMAKRISHNAN and G. ARULDHAS, *J. Solid State Chem.* **66** (1987) 235.
10. G. FERRARIS, D. W. JONES and J. YERKESS, *J. Chem. Soc. Dalton* (1973) 816.
11. E. W. WASHBURN, *Proc. Nat. Acad. Sci.* **7** (1927) 115.
12. R. T. PABALAN and K. S. PITZER, *Geochim. Cosmochim. Acta* **51** (1987) 2429.
13. G. J. KENNEDY, S. L. LAWTON and M. K. RUBIN, *J. Am. Chem. Soc.* **116** (1994) 11000.
14. X. YANG, *J. Phys. Chem.* **99** (1995) 1276.
15. L. W. BECK and J. F. HAW, *ibid.* **99** (1995) 1076.
16. S. C. KOHN, R. DUPREE and M. E. SMITH, *Nature* **337** (1989) 539.
17. I. TKAC, P. KOMADEL and D. MULLER, *Clay Mineral.* **29** (1994) 11.
18. J. ROCHA and J. D. PEDROSA DE JESUS, *ibid.* **29** (1994) 287.
19. C. E. BRONNIRNANN, R. C. ZEIGLER and G. E. MACIEL, *J. Am. Chem. Soc.* **110** (1988) 2023.

Received 10 June
and accepted 30 October 1996